高等学校化学学报
CHEMICAL JOURNAL OF CHINESE UNIVERSITIES
研究论文

自组装纳米胶束通过增加药物积累和延长滞留时间用于肿瘤光动力治疗

安要龙，李子恒，吴富根
（数字医学工程全国重点实验室，江苏省生物材料与器件重点实验室，
东南大学生物科学与医学工程学院，南京 211189）

摘要 通过两亲性*D*-α-生育酚聚乙二醇1000琥珀酸酯(TPGS)和疏水性光敏剂焦脱镁叶绿酸a(Ppa)的共组装制备了用于光动力疗法(PDT)的纳米胶束(表示为TPGS/Ppa). 所制备的纳米胶束为直径(18.0±2.2) nm的球形结构，zeta电位约为−18 mV. 此外，纳米胶束表现出优异的光稳定性、生物相容性和光毒性，并通过增强渗透和滞留效应(EPR效应)有效地到达肿瘤区域. 此外，发现TPGS/Ppa纳米胶束对4T1小鼠乳腺癌细胞的光毒性比游离Ppa更高; 并在4T1荷瘤小鼠模型中验证了该纳米胶束的优异抗肿瘤效果. 本研究开发的新型光动力纳米胶束TPGS/Ppa可增加药物在肿瘤区域的积累并延长其保留时间，为小分子疏水性药物的递送和肿瘤PDT提供了可行的策略.

关键词 光动力疗法; 纳米药物; 光敏剂; *D*-α-生育酚聚乙二醇1000琥珀酸酯; 细胞凋亡
中图分类号 O644.12 **文献标志码** A doi：10.7503/cjcu20240331

A Self-assembled Nanomicelle for Realizing Tumor Photodynamic Therapy *via* Increasing Drug Accumulation and Prolonging Retention Time

AN Yaolong, LI Zi-Heng, WU Fu-Gen*
(*State Key Laboratory of Digital Medical Engineering*, *Key Laboratory for Biomaterials and Devices of Jiangsu Province*, *School of Biological Science and Medical Engineering*, *Southeast University*, *Nanjing* 211189, *China*)

Abstract A nanomicelle(denoted as TPGS/Ppa) was fabricated *via* the coassembly of the amphiphilic *D*-α-tocopheryl polyethylene glycol 1000 succinate (TPGS) and the hydrophobic photosensitizer pyropheophorbide a (Ppa) for photodynamic therapy (PDT). The obtained nanomicelle possessed a spherical structure with a diameter of (18.0±2.2) nm and a zeta potential of approximately −18 mV. Besides, the nanomicelle exhibited excellent photostability, biocompatibility, and phototoxicity, and could effectively reach the tumor region *via* the enhanced permeability and retention effect. Additionally, it could be found that the TPGS/Ppa nanomicelle exhibited higher phototoxicity against 4T1 murine mammary cancer cells than free Ppa. In the 4T1 tumor-bearing mouse model, the nanomicelle showed an excellent antitumor therapeutic effect. This study develops a new type of photodynamic nanomicelle TPGS/Ppa, which can increase the accumulation of drugs and prolong their tumor retention time, providing a feasible strategy for realizing the delivery of small-molecule hydrophobic drugs and tumor PDT.

收稿日期：2024-07-01. 网络首发日期：2024-10-23.
联系人简介：吴富根, 男, 博士, 教授, 主要从事生物材料和纳米药物方面的研究. E-mail: wufg@seu.edu.cn
基金项目：国家自然科学基金(批准号：82372127)资助.
Supported by the National Natural Science Foundation of China (No.82372127).

Keywords Photodynamic therapy; Nanodrug; Photosensitizer; *D*-α-Tocopheryl polyethylene glycol 1000 succinate; Cell apoptosis

1 Introduction

The three fundamental components of photodynamic therapy (PDT) encompass light, photosensitizer (PS), and oxygen[1]. Upon illumination with a particular wavelength of light, the PS embedded in the tumor tissue absorbs energy and initiates photochemical reactions that generate reactive oxygen species (ROS)[2,3]. The resulting ROS induce oxidative stress within the tumor cells, compromising their membranes and leading to cellular destruction and damage[2,3]. Over the past decades, as a noninvasive method for treating tumors, PDT has made significant progress in the treatment of various cancers, including cancers of lung, bladder, head and neck, esophagus, pancreas, and prostate[4]. PDT provides several advantages in anticancer treatment[5—8]. First, PDT rapidly generates ROS within a short time. Second, PSs only produce ROS that induce cell apoptosis after exposure to light, which can thus realize the precise control over the time and location of light exposure to minimize toxicity to healthy tissues. Third, PDT can detect and treat microscopic lesions that are not visible to the naked eye during surgery. Last, PDT can be effectively combined with other therapies such as chemotherapy, radiotherapy, and gene therapy, providing targeted and minimally invasive treatment options for cancer patients[9].

Pyropheophorbide a (Ppa), as a widely used PS in PDT, has found limited clinical applications due to its poor water solubility, aggregation-induced fluorescence quenching, and lack of selectivity for target cells[10,11]. To address these challenges, we use *D*-α-tocopheryl polyethylene glycol 1000 succinate (TPGS, a Food and Drug Administration-approved biocompatible excipient[12] and a derivative of vitamin E) as a carrier for solving the problem of the poor water solubility of Ppa. TPGS has a unique amphiphilic structure with a hydrophilic polyethylene glycol segment and a lipophilic vitamin E moiety. Its hydrophilic-lipophilic balance of 13.2 and low critical micelle concentration (CMC) of 0.02% (or 0.02 mmol/L) make it an ideal solubilizer and emulsifier in drug delivery systems[12]. TPGS can reduce the activity of P-glycoprotein (P-gp) ATPase[13,14], thereby reversing multidrug resistance (MDR) mediated by P-gp[15—17]. This contributes to increased drug concentration within multidrug-resistant cancer cells, enhancing anticancer therapeutic efficacy[18,19]. TPGS can also serve as a drug penetration enhancer to facilitate drug permeation through the skin, gastrointestinal mucosa, or cornea[20—22], which is crucial for drug absorption and treatment effectiveness. Besides, TPGS plays a significant role in the production of ROS and the apoptosis of cancer cells[23]. TPGS may also have the potential to suppress tumor metastasis by downregulating proteins associated with tumor migration, such as matrix metalloproteinase-9[24], Snail[24], epidermal growth factor receptor[25], Twist[26], and urokinase-type plasminogen activator[27]. Therefore, as a safe and effective drug carrier, TPGS is widely used to improve drug efficacy, reverse MDR, and inhibit tumor metastasis.

In this work, to improve tumor targeting efficiency and PDT efficacy of Ppa, we construct a tumor-penetrating and TPGS-enhanced antitumor nanomicelle for realizing the targeted delivery of the PS (Ppa) into the tumor microenvironment, thereby achieving effective PDT. In this research, TPGS serves as the carrier of the hydrophobic small-molecule Ppa, which is encapsulated within the TPGS micelle *via* self-assembly, while Ppa can generate ROS under an appropriate light irradiation condition to effectively kill tumor cells (Scheme 1). This study develops the TPGS/Ppa nanomicelle which can increase the accumulation of drugs and prolong their retention time in the tumor region, providing a feasible strategy for the delivery of small-molecule hydrophobic drugs and tumor PDT.

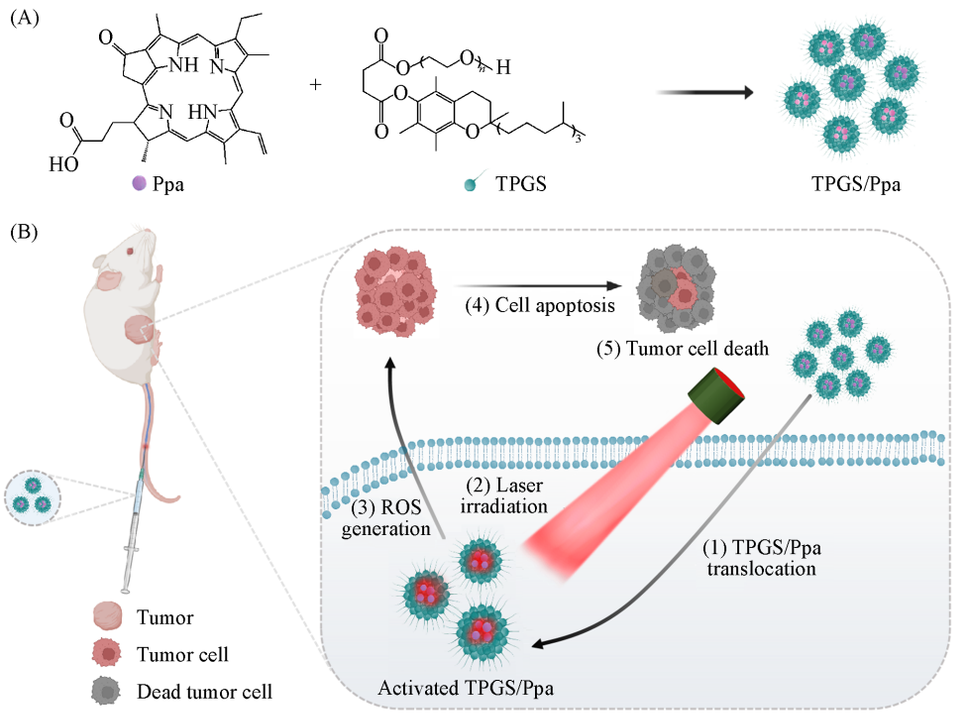

Scheme 1 Scheme illustrating the fabrication of TPGS/Ppa nanomicelle(A) and its application for antitumor PDT(B)

2 Experimental

2.1 Materials and Measurements

Dimethyl sulfoxide(DMSO), TPGS, genistein, and 5-(*N*,*N*-dimethyl)amiloride hydrochloride(amiloride) were obtained from Aladdin Chemistry Co., Ltd.(Shanghai, China). Ppa was purchased from Frontier Scientifc, Inc. Chloroform($CHCl_3$), disodium hydrogen phosphate(Na_2HPO_4), sodium dihydrogen phosphate(NaH_2PO_4), hydrochloric acid(HCl), and ethanol were bought from Sinopharm Chemical Reagent Co., Ltd.(Shanghai, China). Dulbecco's modified Eagle's medium(DMEM), 4T1 mouse breast cancer cells, endoplasmic reticulum(ER)-Tracker Green(ER-Tracker), and rhodamine 123(Rhod 123) were ordered from KeyGen Biotech Co., Ltd.(Nanjing, China). Fetal bovine serum(FBS), 0.25% trypsin-ethylenediaminetetraacetic acid disodium salt dihydrate(0.25% trypsin-EDTA), and LysoTracker Green(LysoTracker) were obtained from Thermo Fisher Scientific, Inc.(USA). 3-(4,5-Dimethyl-2-thiazolyl)-2,5-diphenyl-2*H*-tetrazolium bromide(MTT) was purchased from Heowns(Tianjin, China). Dichlorodihydrofluorescein diacetate(DCFH-DA) was from Beyotime Institute Biotechnology(Shanghai, China). Chlorpromazine hydrochloride(CPZ) and methyl-β-cyclodextrin(MβCD) were bought from Sigma-Aldrich(Shanghai, China). Phosphate-buffered solution(PBS) was obtained from Servicebio Technology Co., Ltd.(Wuhan, China).

The size and morphology of the TPGS/Ppa nanomicelle were characterized using a transmission electron microscope(JEM2100, JEOL Ltd., Japan). The hydrodynamic size and zeta potential of TPGS/Ppa were measured by a zetasizer instrument(Nano ZS, Malvern Instruments, UK). The ultraviolet-visible(UV-Vis) absorption spectra of Ppa and TPGS/Ppa were obtained by using a Shimadzu UV-2600 spectrophotometer. Fluorescence spectra of Ppa and TPGS/Ppa were obtained using a spectrofluorophotometer(RF-5301PC, Shimadzu, Japan). UV-Vis absorption spectra of Ppa and TPGS/Ppa under 671 nm laser continuous illumination(1 mW/cm^2) were recorded using a Shimadzu UV-2600 spectrophotometer. The surface tension values of TPGS at various concentrations were measured using an optical tensiometer(Theta Lite, Biolin Scientific).

2.2 Preparation of TPGS/Ppa Nanomicelle

To prepare the TPGS/Ppa nanomicelle, 0.53 mg of Ppa and 15.13 mg of TPGS (with a Ppa/TPGS molar ratio of 1∶10) were separately dissolved in 300 μL of chloroform. The mixtures were thoroughly dissolved within a test tube using ultrasound and vortex oscillation. Subsequently, the fully dissolved Ppa and TPGS solutions were combined, and further mixed using ultrasound and vortex oscillation. Next, nitrogen gas was used to evaporate the chloroform from the mixture until a non-flowing film formed at the bottom of the test tube. The resulting film was then vacuum-dried overnight to remove residual organic solvent. Finally, the obtained TPGS/Ppa was dissolved in 1 mL of deionized water. All the sample preparation steps were conducted at room temperature.

3 Results and Discussion

3.1 Fabrication and Characterization of TPGS/Ppa Nanomicelles

TPGS/Ppa nanomicelles were prepared using TPGS and Ppa *via* a self-assembly method. The transmission electron microscopy (TEM) image and the corresponding statistical histogram [Fig. 1(A)] revealed that the TPGS/Ppa nanomicelles had a spherical structure with a diameter of (18.0±2.2) nm. Dynamic light scattering (DLS) revealed that the hydrodynamic size and polydispersity index (PDI) of the nanomicelles were (32.9±10.9) nm and 0.502, respectively [Fig. 1(B)]. The hydrodynamic size of TPGS/Ppa is larger than

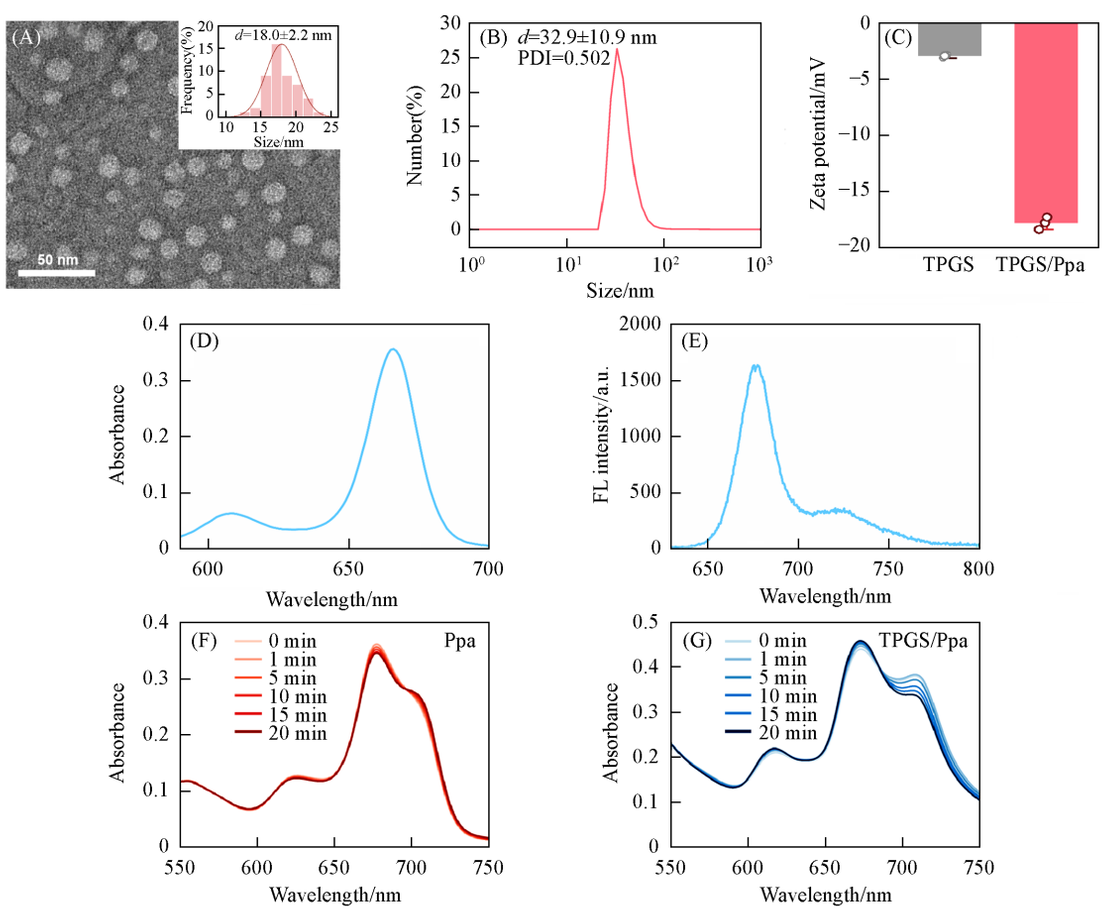

Fig. 1 TEM image and corresponding size distribution histogram of TPGS/Ppa nanomicelles(A), hydrodynamic size and PDI value of TPGS/Ppa nanomicelles measured by DLS(B), zeta potentials of TPGS and TPGS/Ppa(in PBS, pH 7.4)(C), UV-Vis absorption spectrum of TPGS/Ppa(in DMSO)(D), fluorescence emission spectrum(λ_{ex}=608 nm) of TPGS/Ppa(in DMSO)(E), UV-Vis absorption spectra of Ppa(F) and TPGS/Ppa (G)(in PBS with 1% DMSO) under continuous laser irradiation(671 nm and 1 mW/cm^2)

that obtained from TEM, which may be attributed to the presence of a hydration layer of the micelle. The zeta potential of the TPGS/Ppa nanomicelles was approximately −18 mV[Fig.1(C)], and its absolute value was higher than that of TPGS[Fig.1(C)]. The negative zeta potential of the nanomicelles was probably due to the presence of the carboxyl group of Ppa.

The UV-Vis absorption of TPGS/Ppa(in DMSO)[Fig.1(D)] revealed the presence of an absorption peak at ~670 nm attributed to Ppa[28]. The fluorescence emission spectrum of TPGS/Ppa(in DMSO) indicated that the maximum emission wavelength was 678 nm[Fig.1(E)]. To observe the photostability of Ppa and TPGS/Ppa nanomicelles, we performed the continuous illumination (671 nm, 1 mW/cm^2) and measured the absorbance of the Ppa and TPGS/Ppa suspensions in the UV-Vis region. The photostability curves of Ppa and TPGS/Ppa are shown in Fig.1(F) and (G). After 20 min of continuous laser irradiation, there was no significant change in the absorbance of Ppa and TPGS/Ppa samples, indicating that they would not cause significant photobleaching after 20 min illumination, which was beneficial for tumor PDT. Next, we confirmed that TPGS/Ppa was stable after storage in PBS at room temperature for at least 7 days, since during the 7-day storage period, no significant change in hydrodynamic diameter was observed[Fig.S1(A), see the Supporting Information of this paper]. Meanwhile, TPGS/Ppa also exhibited good stability in serum at room temperature for 4 days[Fig.S1(B)].

3.2 Biocompatibility, Cellular ROS Generation and Cellular Uptake of TPGS/Ppa Nanomicelles

To evaluate the cytotoxicity of TPGS, Ppa, and TPGS/Ppa, an MTT assay was conducted, and the results are shown in Fig.2(A) and (B). Without laser irradiation, as the drug concentration increased, the cell survival rates of both TPGS and Ppa groups did not have noticeable changes[Fig.2(A)], indicating the low cytotoxicity of the two reagents. As the drug concentration increased, the cell survival rate of TPGS/Ppa gradually decreased. For example, when the concentration of Ppa(in the TPGS/Ppa group) was 0.5 μmol/L, the cell survival rate was *ca.* 75%, and when the concentration of Ppa(in the TPGS/Ppa group) was 1 μmol/L, the cell survival rate was already below 50%. Under laser irradiation, as the drug concentration increased, the cytotoxicity of TPGS did not show a significant change[Fig.2(B)]. However, as the drug concentration increased, the cell survival rates of Ppa and TPGS/Ppa significantly decreased. Specifically, when the concentration of Ppa was 0.5 μmol/L, the cell survival rate of TPGS was *ca.* 94%, while that of Ppa and TPGS/Ppa was *ca.* 82% and *ca.* 6%, respectively, indicating that the cytotoxicity of TPGS/Ppa was significantly higher than those of Ppa and TPGS under laser illumination.

To investigate the ROS levels of the TPGS-, Ppa-, and TPGS/Ppa-treated 4T1 cells[Fig.2(C)] under laser irradiation, we further employed the 2′,7′-dichlorodihydrofluorescein diacetate cellular ROS detection assay. The results demonstrated that the TPGS/Ppa-treated cells exhibited significantly a higher ROS level compared with either the TPGS-treated cells or the Ppa-treated cells under laser illumination. Besides, under laser conditions, the ROS level of Ppa-treated cells was higher than that of TPGS-treated cells or untreated cells, as Ppa could produce ROS under laser irradiation. These findings suggested that TPGS/Ppa and Ppa could induce cell apoptosis by elevating intracellular ROS levels in the cells. To investigate cellular uptake behavior and determine the optimal drug incubation time for subsequent cellular experiments, we separately studied the cellular uptake behavior of Ppa and TPGS/Ppa[Fig.2(D)—(F)]. From Fig.2(D) and (F), we could see that Ppa reached its highest fluorescence intensity at 3 h and the fluorescence gradually decreased over the next 21 h. Similarly, Fig.2(E) and (F) showed that TPGS/Ppa reached its first fluorescence peak at 4 h, followed by a slight decrease in fluorescence intensity, and then a slow upward trend of the fluorescence change. These results indicated that TPGS could enhance the cellular uptake of Ppa, possibly due to its role as a P-gp inhibitor, which can suppress drug efflux. In addition, different cellular uptake amounts of free Ppa

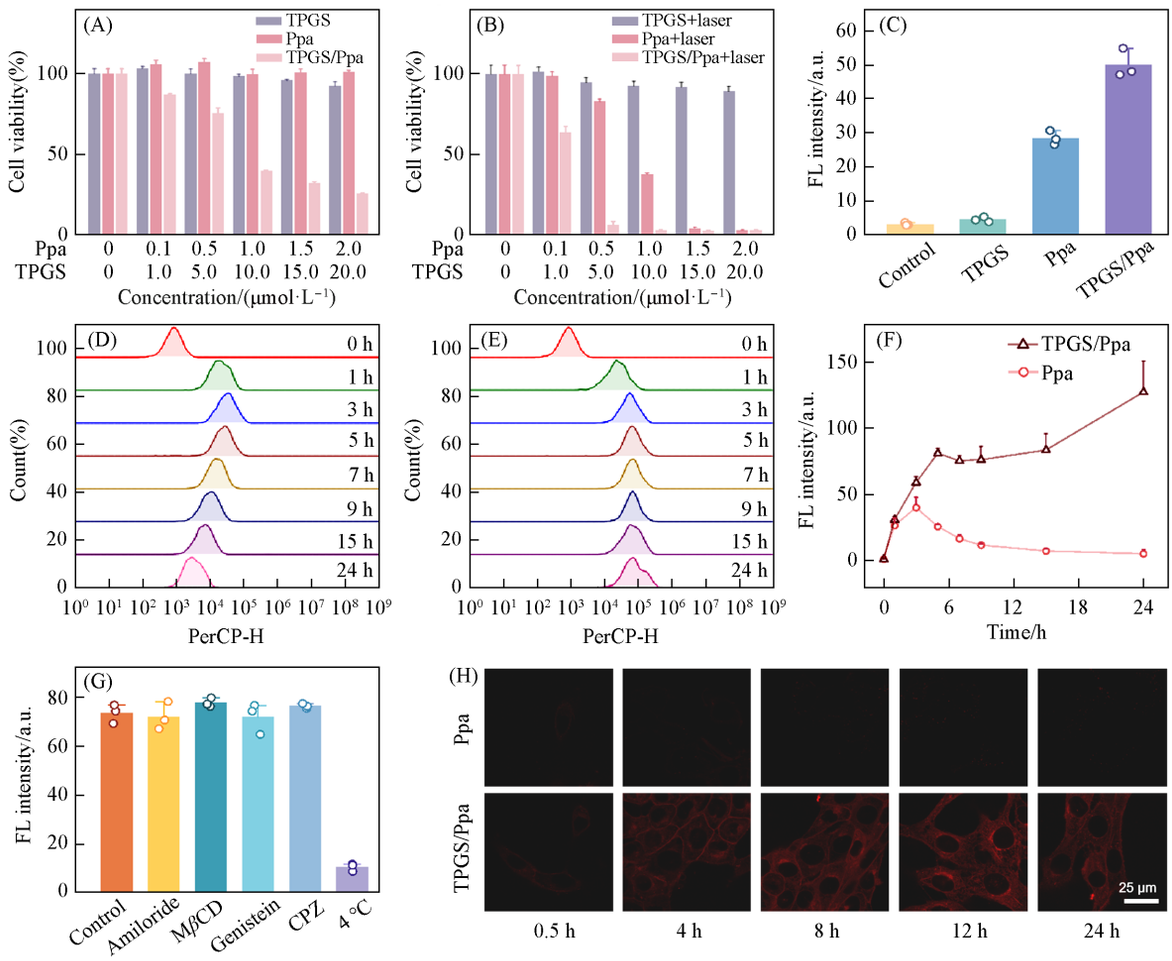

Fig. 2 Relative viabilities of the 4T1 cells treated with different concentrations of TPGS, Ppa, or TPGS/Ppa for 24 h under dark(A) and laser conditions(660 nm, 2 mW/cm², 2 min)(B); ROS levels of TPGS-, Ppa-, or TPGS/Ppa-treated 4T1 cells under laser condition(Ppa=0.5 μmol/L, laser: 660 nm, 2 mW/cm², 1 min)(C); fluorescence intensities of the 4T1 cells incubated with Ppa(D) or TPGS/Ppa(E) for different periods as measured by flow cytometry; fluorescence intensity–time curves of the 4T1 cells incubated with Ppa or TPGS/Ppa for different periods(Ppa=2 μmol/L)(F); flow cytometric results of the 4T1 cells that were treated with culture medium(control), TPGS/Ppa+one endocytic inhibitor(amiloride, MβCD, genistein, or CPZ), or TPGS/Ppa under 4 ℃(G); and confocal fluorescence images of the 4T1 cells after incubation with Ppa or TPGS/Ppa(Ppa=2 μmol/L) for various periods as indicated(H)

and Ppa in TPGS/Ppa may be due to their different cellular uptake mechanisms. To investigate the cellular uptake mechanisms of drugs, we treated the cells with one of the four common endocytic inhibitors (*i. e.*, amiloride hydrochloride, MβCD, genistein, and CPZ) at 37 ℃ or conducted the cellular uptake experiment at 4 ℃[Fig.2(G)]. Notably, the fluorescence intensity of TPGS/Ppa-treated cells at 4 ℃ was significantly lower than that of the untreated group(control), indicating the reduced drug uptake at this temperature, which was possibly due to the decreased cellular activity. The above 4 ℃ treatment experiment revealed that the endocytosis of TPGS/Ppa was energy-dependent. Interestingly, the fluorescence of the TPGS/Ppa-treated cells did not exhibit significant changes when coincubated with one of the four endocytic inhibitors. This suggested that the TPGS/Ppa nanomicelles did not rely on macropinocytosis-, lipid raft-, caveolae-, or clathrin-mediated endocytosis to enter the 4T1 cells. Thus, we hypothesize that TPGS/Ppa employs an alternative pathway for cellular internalization beyond the aforementioned pathways. To visualize the cellular uptake behavior more intuitively, we observed the intracellular fluorescence of Ppa and TPGS/Ppa at different time points using

confocal fluorescence microscopy[Fig.2(H)]. Based on the confocal imaging results, both TPGS/Ppa nanomicelles and free Ppa exhibited an increase in fluorescence intensity within 24 h in 4T1 cells. At an equivalent Ppa concentration and the same incubation time, TPGS/Ppa showed a slightly higher fluorescence intensity compared with free Ppa, further demonstrating that TPGS could enhance the cellular internalization of Ppa to some extent.

3.3 Intracellular Distribution and Cell Apoptosis Assay

To further investigate the intracellular localization of Ppa and TPGS/Ppa and explore whether they can target certain cellular organelles, ER-Tracker, LysoTracker, and Rhod 123 were separately introduced to the 4T1 cells to visualize the ER (Fig. 3), lysosome (Fig. 4), and mitochondrion (Fig. 5), respectively.

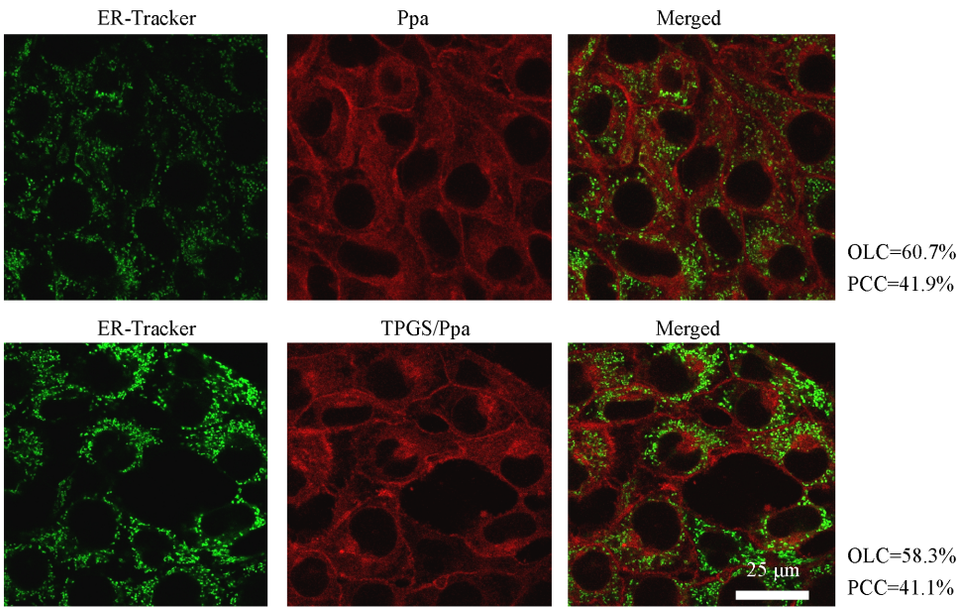

Fig. 3 Confocal fluorescence images of Ppa- or TPGS/Ppa-treated 4T1 cells stained with ER-Tracker

The images in the last column illustrate the intensity correlations of Ppa (or TPGS/Ppa) and ER-Tracker.

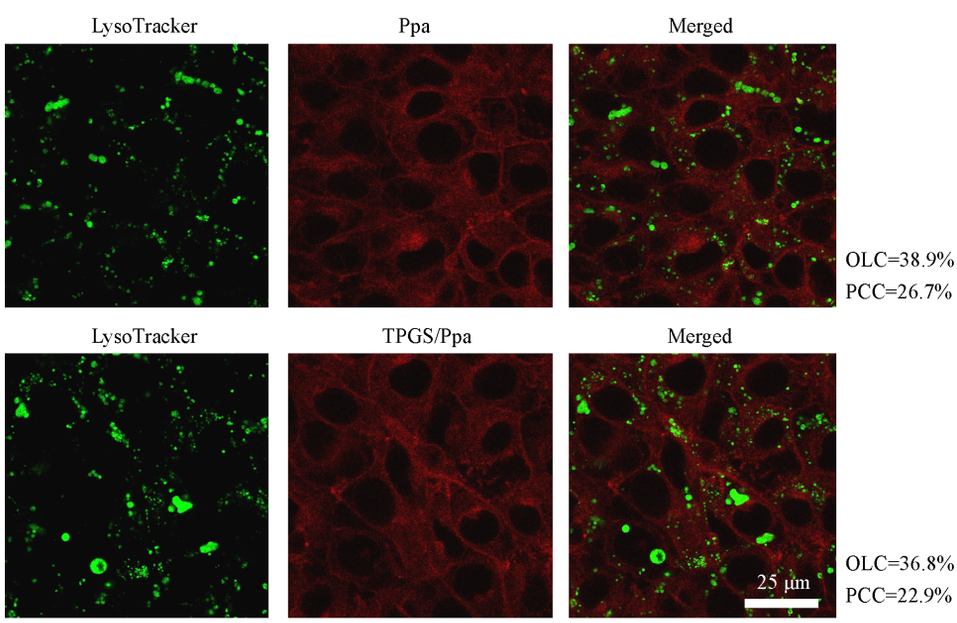

Fig. 4 Confocal fluorescence images of Ppa- or TPGS/Ppa-treated 4T1 cells stained with LysoTracker

The images in the last column illustrate the intensity correlation of the Ppa (or TPGS/Ppa) and LysoTracker.

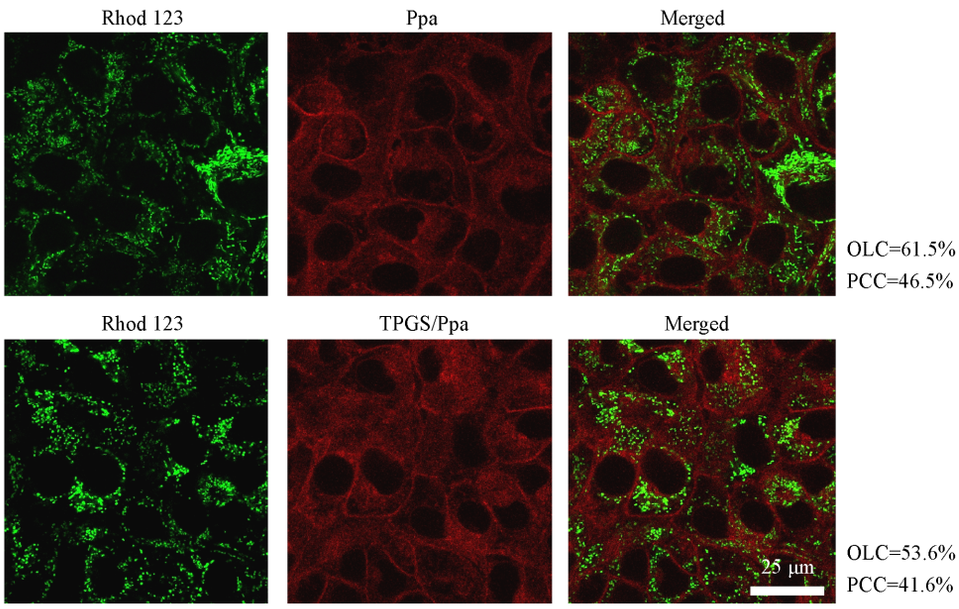

Fig. 5 Confocal fluorescence images of Ppa- or TPGS/Ppa-treated 4T1 cells stained with Rhod 123

The images in the last column illustrate the intensity correlation of the Ppa(or TPGS/Ppa) and Rhod 123.

Additionally, we analyzed the Pearson's correlation coefficient(PCC) and overlap coefficient(OLC) of Ppa(or TPGS/Ppa) with ER, lysosome, and mitochondrion. The PLC and OLC values indicated that there was no significant colocalization of Ppa(or TPGS/Ppa) with ER, lysosome, and mitochondrion.

To investigate the impact of TPGS/Ppa or Ppa on cell apoptosis under laser and dark conditions, we conducted the annexin V-fluorescein isothiocyanate(FITC)/propidium iodide(PI) dual staining assay(Fig.6). According to the results of the apoptosis assay, TPGS/Ppa significantly induced cell apoptosis under laser conditions. Compared with the single drug, TPGS/Ppa caused a higher apoptotic rate of cells under laser exposure. Some cells were in the early apoptotic stage due to insufficient post-illumination incubation time or inadequate duration of laser exposure.

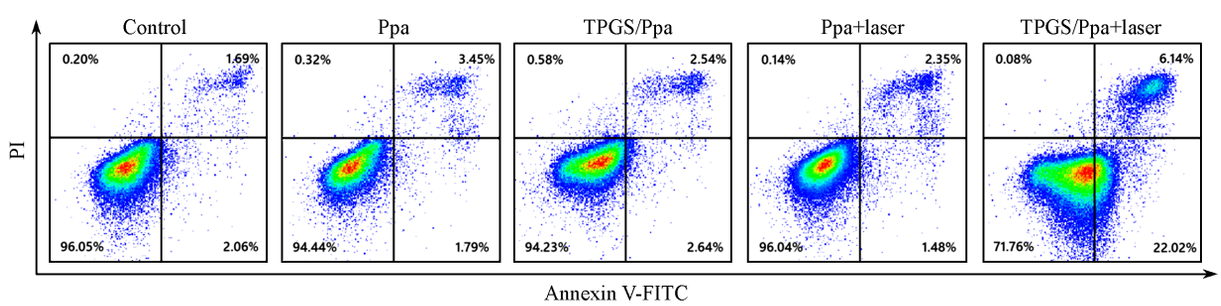

Fig. 6 Flow cytometric results of 4T1 cells after treatment with culture medium(control), Ppa, TPGS/Ppa, Ppa+laser, or TPGS/Ppa+laser(660 nm, 2 mW/cm^2, 1 min)

After drug/laser treatment, the cells were subjected to the annexin V-FITC/PI dual staining.

3.4 Intracellular Distribution and Cell Apoptosis Assay

We further conducted animal experiments to investigate the distribution of drugs in various major organs and the tumor regions. After intravenous (i. v.) injection of TPGS/Ppa or Ppa, the 4T1 tumor-bearing mice were euthanized at 0 h, 6 h, 12 h, 24 h, 3 d, and 7 d[Fig.7(A)]. The tumors, hearts, kidneys, livers, spleens, and lungs were dissected, and the fluorescence intensity of each tissue was measured by flow cytometry. To conduct subsequent *in vivo* therapeutic experiments in the mice, we investigated the distribution of TPGS/Ppa or Ppa in various major organs and the tumor regions at different time points

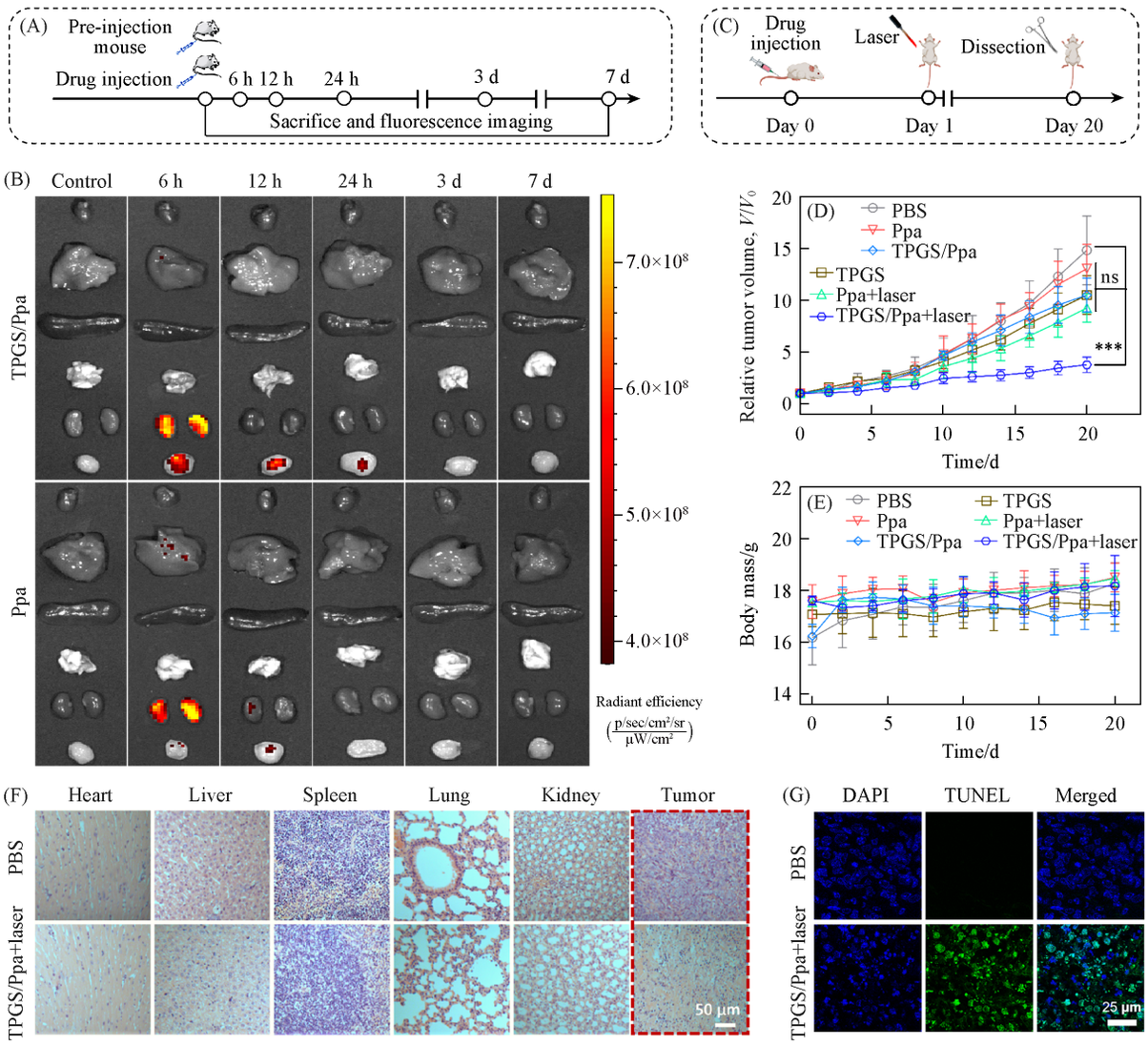

Fig. 7 Timeline of the *in vivo* therapeutic evaluation experiments(A), *ex vivo* fluorescence images of tumor tissues and major organs of the 4T1 tumor-bearing mice sacrificed before injection(control) and at different time points after i. v. injection with Ppa or TPGS/Ppa(Ppa=4 mg/kg) (B), experimental outline of various treatment steps for evaluating the anticancer efficiencies of different drugs in tumor-bearing mice(C), relative tumor volumes(D) and body weights of the tumor-bearing mice after different treatments(E), H&E-stained tissue slices of major organs(hearts, livers, spleens, lungs, and kidneys) and tumors of the mice sacrificed on the 20th day after treatment with PBS or "TPGS/Ppa+laser"(F), TUNEL assay results of the tumor tissues collected from the mice after treatment with PBS or "TPGS/Ppa+laser"(G)

(B) From top to bottom in each image: heart, liver, spleen, lung, kidneys, and tumor; (C) for phototherapy, 671 nm laser irradiation (15 mW/cm^2, 15 min) was carried out at 1 d after i.v. injection of Ppa and TPGS/Ppa (Ppa=4 mg/kg); (D) statistical significance was calculated *via* one-way analysis of variance (ANOVA) with a Tukey's post-hoc test. The P values of less than 0.05 were considered significant. ***$P < 0.001$; ns: non-significant difference. (D, E) The statistical data were expressed as mean±standard deviation (n=3).

[Fig.7(B)]. The results revealed that the TPGS/Ppa group exhibited a higher fluorescence intensity in the tumor regions at 6, 12, and 24 h compared with the group treated with Ppa alone, indicating better tumor accumulation in the TPGS/Ppa group. Additionally, the experimental results demonstrated that TPGS/Ppa still exhibited fluorescence in the tumor region at 24 h after injection, whereas there was no fluorescence in the Ppa group, suggesting that compared with free Ppa, TPGS/Ppa exhibited higher drug accumulation

and longer retention time in the tumor region. Besides, TPGS/Ppa did not show fluorescence in the tumor region at 3 and 7 d, implying that TPGS/Ppa was completely cleared within 3 days, indicating its excellent biosafety.

To investigate the antitumor PDT efficacy of TPGS/Ppa, we conducted *in vivo* therapeutic evaluations in mice[Fig.7(C)]. Based on the treatment results, there were no significant differences in the tumor volume among the PBS group, TPGS group, Ppa group, TPGS/Ppa group, and "Ppa+laser" group[Fig.7(D)]. However, the tumor volume in the "TPGS/Ppa+laser" group was lower than the tumor volumes in the other groups, suggesting that "TPGS/Ppa+laser" can markedly inhibit tumor growth. Additionally, the body weight of the mice in each group did not show significant changes[Fig.7(E)], suggesting that none of the therapeutic strategies elicited severe adverse effects. To investigate the impact of TPGS/Ppa on various organs in mice, we collected the main organs (including hearts, livers, spleens, lungs, kidneys, and tumors) from the mice treated with PBS or "TPGS/Ppa+laser", and performed hematoxylin and eosin (H&E) staining for the tissue slices from these organs[Fig.7(F)]. The results revealed that in the "TPGS/Ppa+laser" group, the tumor region in the mice exhibited significant cell damage due to the drug treatment and laser exposure. However, the structures of the organs such as the heart, liver, spleen, lung, and kidney in the mice remained normal, implying that TPGS/Ppa exhibited excellent biocompatibility. To investigate the biological mechanism underlying the inhibition of tumor growth by TPGS/Ppa+laser, we performed terminal deoxynucleotidyl transferase-mediated dUTP nick-end labeling (TUNEL) assay on the tissues from the "TPGS/Ppa+laser" group of mice[Fig.7(G)]. We compared the TUNEL assay results of the tissue slices from the PBS and "TPGS/Ppa+laser" groups to explore the impact of "TPGS/Ppa+laser" treatment on cellular apoptosis at the tissue level. In the "TPGS/Ppa+laser" group, the tumor region in the mice exhibited abundant green fluorescence, indicating significant DNA damage and exposure of 3′-OH ends[29] (which are typical characteristics of apoptotic cells). Additionally, the green fluorescence was more pronounced at the nuclear membrane periphery than at other regions, consistent with the characteristic chromatin condensation near the nuclear membrane in apoptotic cells. In contrast, the PBS group showed almost no green fluorescence, suggesting that this group consisted primarily of viable cells. In summary, the results of the TUNEL assay provided evidence that "TPGS/Ppa+laser" treatment could effectively inhibit tumor growth by inducing apoptosis in tumor cells.

4 Conclusions

TPGS/Ppa nanomicelles with excellent photostability, biocompatibility, and phototoxicity were prepared *via* the self-assembly of TPGS and Ppa for realizing antitumor PDT, providing a new way for the delivery of small-molecule hydrophobic drugs. The obtained TPGS/Ppa nanomicelle exhibits low cytotoxicity under dark conditions, but shows significantly enhanced cytotoxicity under laser exposure. Compared with free Ppa, TPGS/Ppa demonstrates higher intracellular uptake in 4T1 tumor cells. Moreover, under laser exposure, TPGS/Ppa generates a substantial amount of ROS, effectively inducing cell apoptosis and achieving efficient tumor cell destruction. Furthermore, *in vivo* therapeutic experiments demonstrate that TPGS/Ppa shows enhanced drug accumulation and prolonged retention in the tumor region, and can thus achieve efficacious antitumor PDT *in vivo*. Finally, since the PS loaded in the nanomicelle possesses both photoresponsive and sonoresponsive properties, we believe that such a nanomicelle may also hold the potential for realizing sonodynamic therapy to overcome the poor light penetration issue.

The supporting information of this paper see http://www.cjcu.jlu.edu.cn/CN/10.7503/cjcu20240331.

参 考 文 献

[1] Agostinis P., Berg K., Cengel K. A., Foster T. H., Girotti A. W., Gollnick S. O., Hahn S. M., Hamblin M. R., Juzeniene A., Kessel D., Korbelik M., Moan J., Mroz P., Nowis D., Piette J., Wilson B. C., Golab J., *CA-Cancer J. Clin.*, **2011**, *61*(4), 250—281
[2] Choi J., Sun I. C., Hwang H. S., Yoon H. Y., Kim K., *Adv. Drug Delivery Rev.*, **2022**, *186*, 114344
[3] Bai F., Deng Y., Li L., Lv M., Razzokov J., Xu Q., Xu Z., Chen Z., Chen G., Chen Z., *Exploration*, **2024**, DOI: 10.1002/EXP.20230177
[4] Overchuk M., Weersink R. A., Wilson B. C., Zheng G., *ACS Nano*, **2023**, *17*(9), 7979—8003
[5] Cheong T. C., Shin E. P., Kwon E. K., Choi J. H., Wang K. K., Sharma P., Choi K. H., Lim J. M., Kim H. G., Oh K., Jeon J. H., So I., Kim I. G., Choi M. S., Kim Y. K., Seong S. Y., Kim Y. R., Cho N. H., *ACS Chem. Biol.*, **2015**, *10*(3), 757—765
[6] Hwang H. S., Shin H., Han J., Na K., *J. Pharm. Invest.*, **2018**, *48*(2), 143—151
[7] Ozog D. M., Rkein A. M., Fabi S. G., Gold M. H., Goldman M. P., Lowe N. J., Martin G. M., Munavalli G. S., *Dermatol. Surg.*, **2016**, *42*(7), 804—827
[8] Wachowska M., Muchowicz A., Demkow U., *Cent. Eur. J. Immunol.*, **2015**, *40*(4), 481—485
[9] Liu Y., Meng X., Bu W., *Coord. Chem. Rev.*, **2019**, *379*, 82—98
[10] Li W., Tan S., Xing Y., Liu Q., Li S., Chen Q., Yu M., Wang F., Hong Z., *Mol. Pharmaceutics*, **2018**, *15*(4), 1505—1514
[11] Xiong H., Yan J., Cai S., He Q., Wen N., Wang Y., Hu Y., Peng D., Liu Y., Liu Z., *Mol. Pharmaceutics*, **2020**, *17*(8), 2882—2890
[12] Tan S., Zou C., Zhang W., Yin M., Gao X., Tang Q., *Drug Delivery*, **2017**, *24*(1), 1831—1842
[13] Collnot E. M., Baldes C., Wempe M. F., Kappl R., Hüttermann J., Hyatt J. A., Edgar K. J., Schaefer U. F., Lehr C. M., *Mol. Pharmaceutics*, **2007**, *4*(3), 465—474
[14] Collnot E. M., Baldes C., Schaefer U. F., Edgar K. J., Wempe M. F., Lehr C. M., *Mol. Pharmaceutics*, **2010**, *7*(3), 642—651
[15] Tang J., Fu Q, Wang Y., Racette K., Wang D., Liu F., *Cancer Lett.*, **2013**, *336*(1), 149—157
[16] Qiu L., Qiao M., Chen Q., Tian C., Long M., Wang M., Li Z., Hu W., Li G., Cheng L., Cheng L., Hu H., Zhao X., Chen D., *Biomaterials*, **2014**, *35*(37), 9877—9887
[17] Qiao H., Zhu Z., Fang D., Sun Y., Kang C., Di L., Zhang L., Gao Y., *J. Drug Targeting*, **2018**, *26*(1), 75—85
[18] Guo Y., Luo J., Tan S., Otieno B. O., Zhang Z., *Eur. J. Pharm. Sci.*, **2013**, *49*(2), 175—186
[19] Choudhury H., Gorain B., Pandey M., Kumbhar S. A., Tekade R. K., Iyer A. K., Kesharwani P., *Int. J. Pharm.*, **2017**, *529*(1/2), 506—522
[20] Fan Z., Wu J., Fang X., Sha X., *Int. J. Pharm.*, **2013**, *445*(1/2), 141—147
[21] Duan Y., Cai X., Du H., Zhai G., *Colloids Surf., B.*, **2015**, *128*, 322—330
[22] Pham C. V., Cho C. W., *J. Pharm. Invest.*, **2017**, *47*(2), 111—121
[23] Neuzil J., Dong L. F., Ramanathapuram L., Hahn T., Chladova M., Wang X. F., Zobalova R., Prochazka L., Gold M., Freeman R., Turanek J., Akporiaye E. T., Dyason J. C., Ralph S. J., *Mol. Aspects Med.*, **2007**, *28*(5/6), 607—645
[24] Xu P., Yin Q., Shen J., Chen L., Yu H., Zhang Z., Li Y., *Int. J. Pharm.*, **2013**, *454*(1), 21—30
[25] Kutty R. V., Chia S. L., Setyawati M. I., Muthu M. S., Feng S. S., Leong D. T., *Biomaterials*, **2015**, *63*, 58—69
[26] Shen J., Sun H., Xu P., Yin Q., Zhang Z., Wang S., Yu H., Li Y., *Biomaterials*, **2013**, *34*(5), 1581—1590
[27] Xu P., Yu H., Zhang Z., Meng Q., Sun H., Chen X., Yin Q., Li Y., *Biomaterials*, **2014**, *35*(26), 7574—7587
[28] Jang B., Choi Y., *Theranostics*, **2012**, *2*(2), 190—197
[29] Sharma R., Iovine C., Agarwal A., Henkel R., *Andrologia*, **2021**, *53*(2), e13738

(Ed.: N, K)